ELSEVIER

Journal of Fluids and Structures 19 (2004) 335–348

JOURNAL OF FLUIDS AND STRUCTURES

www.elsevier.nl/locate/jnlabr/yjfls

# Properties of single shear layer instabilities and vortex-induced excitation mechanisms of thick plates

P. Billeter*,[1]

*IUB Engineering Services Ltd., Thunstrasse 2, P.O. Box CH 3000 Berne 6, Switzerland*

Received 23 April 2001; accepted 15 December 2003

**Abstract**

The basic findings of an experimental investigation of flow-induced vibrations of gate plates with multiple degrees of freedom are presented. The study focused on the fluid dynamic behaviour of the single shear layer separating from a thick rectangular plate. The principal aim of the study was to further the physical understanding of instability-induced excitation mechanisms (IIE) involving shear layer instabilities and vortex generation. It is shown that this type of gate vibration is caused by two dominant excitation mechanisms: cross-flow and streamwise impinging-leading-edge-vortex (ILEV) excitation and streamwise body-resonant leading-edge-vortex-shedding (BR-LEVS) excitation. The first mechanism is caused by the local interaction of the shear layer underneath the gate plate with the trailing edge of the gate lip. The second mechanism is produced by the instability of the shear layer in the tailwater of the gate, with the instability being necessarily triggered by the elastic motion of the flow separation at the leading edge of the gate.


## 1. Introduction

Flow-induced vibrations of gates and valves have practical significance with regard to the safety and the operation reliability of spillways and outlet devices of hydropower plants. Some of the relevant excitation mechanisms are caused by the instability of a single shear layer which separates from the gate and propagates towards the tailwater. Depending on the shape of the gate lip (i.e., the locus of the flow separation), underflown gates with submerged discharge are among the gate types most susceptible to flow-induced vibrations. Therefore, numerous studies investigating these excitation mechanisms were carried out during the last years; see, e.g., Naudascher and Rockwell (1994). A variety of mechanisms was found leading to gate excitation either in the cross-flow or streamwise direction: for cross-flow excitation, see, e.g., Thang (1990), Thang and Naudascher (1986), Kolkman (1976), Hardwick (1974); for streamwise excitation, see, e.g., Jongeling (1988), Thang (1990) and Ishii and Knisely (1990).

Most of the severe flow-induced vibration phenomena belong to two groups of excitation mechanisms. The first group contains the instability-induced excitation mechanisms (IIE) which occur at low or moderate reduced velocities with the vibration velocities nearly as large as the flow velocity. The so-called movement-induced excitation mechanisms (MIE) with vibration velocities much smaller than the flow velocity (large reduced velocities) belong to the second group.

A summary of all excitation mechanisms occurring at underflown gates with two degrees of freedom (2 d.o.f.) and submerged discharge, as shown in Fig. 1 is given in Billeter and Staubli (2000) and Billeter (1998). The gate response to these excitation mechanisms is shown in Fig. 2. As will be pointed out in Section 5.1, the vibration phenomena which

*Tel.: +41-31-357-1260; fax: +41-31-357-1112.

*E-mail address:* peter.billeter@iub-bern.ch (P. Billeter).

[1] Former address. Laboratory of Hydraulics (VAW), Swiss Federal Institute of Technology (ETH), Zurich, Switzerland.

0889-9746/$ - see front matter © 2004 Elsevier Ltd. All rights reserved.
doi:10.1016/j.jfluidstructs.2003.12.008

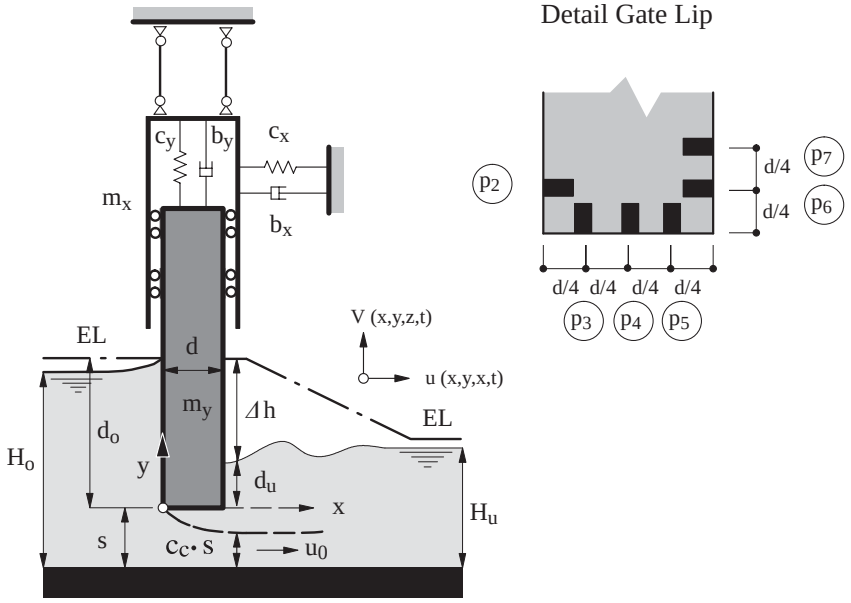


Fig. 1. Schematics and definitions: cross-section and detail of the gate lip.

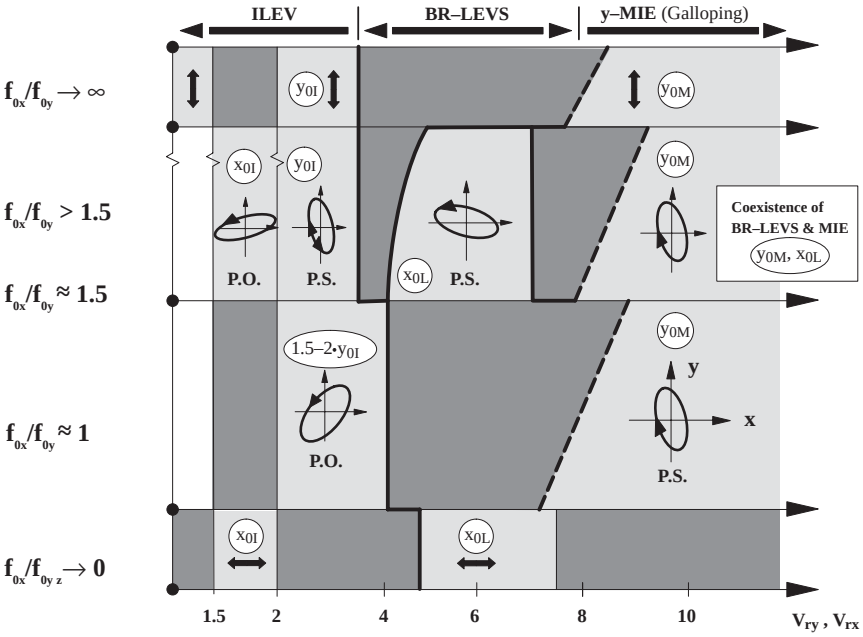


Fig. 2. Motion trajectories and excitation ranges of flow-induced vibrations of gates with 2 d.o.f. [$x_{0I}, y_{0I}, x_{0L}, y_{0M}$ are the reference amplitudes of a gate with 1 d.o.f., P.S./P.O. = press-shut / press-open behaviour of the gate; see Billeter and Staubli (2000)].

occur in a distinct range of gate openings are dominantly influenced by the reduced velocity $V_r$ which represents the ratio between the flow velocity and the vibration velocity and the ratio of the natural frequencies of the gate. The present paper focuses on the fluid-dynamic properties of the IIE mechanisms which occur at low and moderate reduced velocities with $V_r < 8$ (Fig. 2).

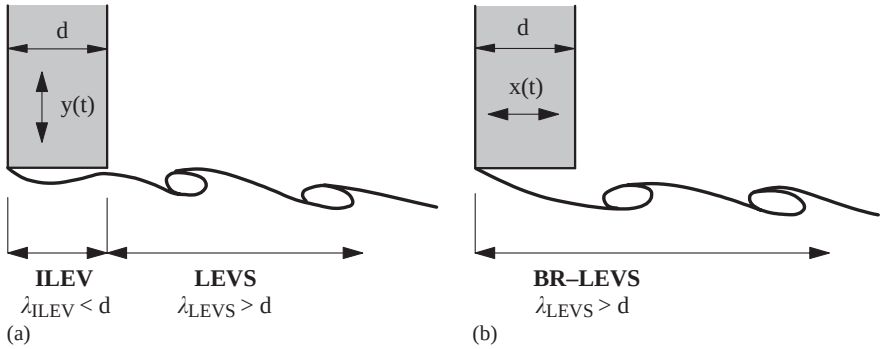


Fig. 3. Excitation mechanisms caused by the instability of a single shear layer separating from an elastic body with 2 d.o.f. (a) cross-flow impinging-leading-edge-vortex (ILEV) excitation; (b) streamwise body-resonant leading-edge-vortex-shedding (BR-LEVS) excitation.

The IIE mechanisms are associated with the instability of shear layers separating from an elastic body and the generation of vortices. Pressure fluctuations caused by these flow structures propagate along the body from which the flow separated and act on the body itself, thus forcing body motions, which in turn affect the flow separation. Consequently, a closed feedback-loop involving the flow separation and the body dynamics occurs. Positive feedback leads to self-excited vibrations with limit-cycle amplitudes given by the structural and fluid-dynamic properties of the system.

Fig. 3 shows typical flow structures of the shear layer beneath the gate lip and in the tailwater of a vibrating gate plate. As will be shown, IIE mechanisms include:

(a) Impinging-leading-edge-vortex (ILEV) excitation, which is produced by the instability of the shear layer between the leading and the trailing edge of the gate lip (Fig. 3(a)), and
(b) Leading-edge-vortex-shedding (LEVS) excitation, which is caused by vortical flow structures in the tailwater of the gate (Fig. 3(b)).

The present paper highlights the characteristic physical properties of both the flow instabilities and the feedback mechanisms involving the gate dynamics. By means of experimental evidence the vortical flow pattern and the flow–structure interaction leading to the IIE of structures with 2 d.o.f. will be thoroughly explained.

## 2. Experimental set-up

The test facility consisted of a vertical gate plate of 1-m height which was positioned in a horizontal laboratory flume of about 10-m length and 1-m width (turbulence level of the undisturbed approach flow: Tu $\approx$ 2%). The gate plate was suspended by a special construction allowing the gate to oscillate both in the cross-flow (vertical) and in the streamwise (horizontal) direction (Fig. 1). The restoring forces were provided by linear springs. Thus, the gate acted as a linear mass oscillator with two perpendicular d.o.f. and two natural frequencies ($f_{0x}$ in streamwise and $f_{0y}$ in cross-flow direction). The gate was underflown and had a rectangular bottom lip shape in order to produce maximum fluid dynamic excitation and to exclude any structural coupling. The width of the gate was $d = 10$ cm.

The gate lip was equipped with miniature pressure transducers which were flush mounted to the structural surface. The position of the pressure transducers can be seen in Fig. 1. The response of the body-oscillator was measured by load- and deflection-cells which were located at or close to the gate suspensions. The signals of all the gauges were amplified by two carrier frequency amplifiers and simultaneously digitized (HBM DMC 9012A, with built-in filters). The data was collected by a Macintosh computer using an IEEE-488 interface. The record length was typically $15 \times 2^{12}$ samples per gauge and the sampling rate was 150 Hz. Applying appropriate FFT-techniques, (overlapping Hamming-windows, blockwise averaging and both frequency and peak power estimation routines), a frequency resolution of about 0.02 Hz and an amplitude resolution better than 0.2 dB was achieved in the frequency domain.

In order to measure the local flow velocities and to investigate the flow field around the gate lip and in the tailwater of the gate, a Dantec-BSA two-component fibre-optic LDA-system was used. For the assessment of the fluid-dynamic excitation mechanism and the relevant flow structures, both simultaneous and synchronized measurements of the body

response, the surface pressure and the local flow velocity were carried out. The experimental set-up and the measurement techniques applied are fully detailed in Billeter (1998).

## 3. Analysis and relevant properties

An extended analysis of the structural dynamics and the excitation forces is given in Billeter (1998) and Billeter and Staubli (2000). To demonstrate the behaviour of the shear layer beneath the gate lip and its significance to gate vibrations, we assume an elliptic trajectory of the gate motion (i.e., an orbit) with the amplitudes $x_i$ and $y_i$ in streamwise and cross-flow direction, respectively:

$$x_i(t) = x_i \sin(\omega_i t), \tag{1a}$$

$$y_i(t) = y_i \sin(\omega_i t + \varphi_i). \tag{1b}$$

The index "$i$" denotes the vibration mode of the system with 2 d.o.f., and becomes "$x$" if the mode in streamwise direction with natural frequency $f_{0x}$ is dominant, and "$y$" if the cross-flow mode with natural frequency $f_{0y}$ dominates the gate response. This simplified approach for the gate response holds for most types of flow-induced gate vibrations detected by Billeter (1998) and Billeter and Staubli (2000). Gate vibrations of the IIE-type only occur at small relative gate openings within the range $0.4 \leqslant s/d \leqslant 1.5$ ($s$ is the width of gate opening and $d$ the thickness of gate lip).

Depending on both the range of reduced velocities $V_{ri} = u_0/(f_i d)$ and the ratio of natural frequencies $f_{0x}/f_{0y}$, either the amplitudes $y_i$ in the vertical direction or the amplitudes $x_i$ in the streamwise direction are dominant. With $y_i$ dominant the frequency $f_i = \omega_i/2\pi$ is close to $f_{0y}$; with $x_i$ dominant the frequency $f_i$ usually lies in the range $0.5f_{0x} < f_i < f_{0x}$. With the phase $\varphi_i$ between $x_i(t)$ and $y_i(t)$ and the ratio $x_i/y_i$, the size and the direction of the principal axis of the elliptic orbit of the gate motion can be determined. Characteristic gate response as a function of the dominant parameters $V_{ri}$ and $f_{0x}/f_{0y}$ are shown in Fig. 2 and explained in more detail in Section 5.

Let the pressure fluctuation $p(x, t)$ along the gate lip be

$$p(x, t) = p_0 e^{j(kx-\omega t)}, \tag{2}$$

with the complex wavenumber $k = k_r + jk_j$ [$k_r$ is the real wavenumber of the convective wave propagation in the $x$ direction, $-k_j$ the spatial growth rate of the pressure wave, $j = (-1)^{0.5}$] and the complex frequency $\omega = \omega_r + j\omega_j$ ($\omega_j$ is the temporal growth rate, which will be neglected and thus $\omega_r = \omega$ are the frequency of the wave propagation). For further analysis, we assume that the frequency of the dominant flow structure causing the vibration phenomenon is equal to the vibration frequency of the gate. The fluctuating pressure related to this flow structure at a distinct position $n$ can thus be described by

$$p_n(t) = p_n \sin(\omega_i t - \varphi_{in}), \tag{3}$$

with $p_n$ being the pressure amplitude, $\omega_i$ the frequency of dominant vibration in $i$ direction and $\varphi_{in}$ the phase shift between the gate deflection in $i$ direction and the pressure at position $n$. The dimensionless pressure amplitude $C'_{pn}$ and the so-called excitation (pressure) coefficient $C^*_{pn}(i)$ are defined as

$$C'_{pn} = 2p_n/(\rho u_0^2), \tag{4a}$$

$$C^*_{pn}(i) = C'_{pn} \sin(-\varphi_{in}), \tag{4b}$$

with $u_0$ being the mean outflow velocity at the vena contracta and $\rho$ the fluid-density. If $C^*_{pn}(i)$ is positive, the vibration in direction $i$ will be sustained by pressure fluctuations at position $n$ (energy transfer from the flow to the structure), and vice versa. If we further assume that Eq. (2) gives a rough estimate for the instantaneous pressure distribution between two positions $n$ and $m$ along the bottom face of the gate, the parameters $\lambda = 2\pi/k_r$ ($\lambda$ the wavelength) and spatial growth rate $k_j$ can be computed for $\lambda_{nm}$ and $-k_{j,nm}$ between the two positions $n$ and $m$ as

$$\lambda_{nm} = 2\pi(\Delta x/\Delta\varphi_{nm}), \tag{5a}$$

$$-k_{j,nm} = (1/\Delta x)\ln(C'_{pm}/C'_{pn}), \tag{5b}$$

with $\varphi_{nm}$ being the phase shift between the pressure at the two positions $n$ and $m$ which are separated by the streamwise distance $\Delta x$. The convection velocity $u_c$ ($= \omega_r/k_r$) of the flow structure which causes $p_n(t)$ and the vibration with frequency $\omega_i$ between the two positions $n$ and $m$ is expressed as

$$u_{c,nm} = \omega_i(\Delta x/\Delta\varphi_{nm}). \tag{5c}$$

In dimensionless form, the key properties wavelength $\lambda_{nm}$, growth rate $-k_{j,nm}$ and convection velocity $u_{c,nm}$ can be written as $\lambda^*_{nm} = \lambda_{nm}/d$ (wavelength normalized by the lip extension), $-k^*_{j,nm} = -k_{j,nm}d$ (relative growth of pressure amplitude along the gate lip extension) and $u^*_{c,nm} = u_{c,nm}/u_0$ (convection velocity normalized by the outflow velocity at the vena contracta). With regard to the suspected excitation by shear layer impingement, we furthermore define a phase condition as

$$d/\lambda = (n + \varepsilon), \tag{5d}$$

with the typical fraction $\varepsilon$ and the number $n$ for the amount of whole wavelengths between the loci of flow separation and impingement (i.e., the gate lip extension $d$).

## 4. Shear layer of the outflow underneath a rigid gate plate

For the assessment of the IIE mechanisms described in Section 5, the behaviour of the outflow from the rigid gate is summarized. Detailed results of the properties of the shear layer beneath the gate at rest are given in Billeter (1998) and Billeter and Staubli (2000). The findings can be summarized as follows.

(i) In the shear layer of the outflow, significant coherent flow structures with distinct frequencies $f_i$ can be detected.
(ii) These structures undergo a vortex pairing process while propagating towards the tailwater of the gate. The frequency $f_i$ of the dominant flow structures decreases step by step with increasing distance from the gate lip.
(iii) The dimensionless frequencies $\mathrm{Sh}_i = f_i d/u_0$ of these structures are typically $\mathrm{Sh}_1 \approx 0.4$, $\mathrm{Sh}_2 \approx 0.2$ and $\mathrm{Sh}_3 \approx 0.1$ with a variation of $\pm 15\%$ depending on the Reynolds number of the outflow. The frequency $\mathrm{Sh}_1$ can be explained by the (linear) stability analysis of (plain) free shear layers (for an overview see Ho and Huerre (1984), an application regarding underflown gates is found in Martin et al., 1975). The $\mathrm{Sh}_1$ corresponds to the fundamental frequency of the flow instability with maximal growth rate.
(iv) The convection velocity $u_c$ of these structures remains rather constant at $u_c/u_0 \approx 0.6$ within the range $0.8 < x/d < 5$ ($x/d = 0$ is the upstream edge of the gate, i.e., the locus of flow separation).

## 5. Properties of the IIE mechanisms

### 5.1. Gate response under investigation

In Fig. 2, the response of underflown gates with 2 d.o.f., rectangular gate lip and submerged discharge is shown (Billeter, 1998). The dominant parameters influencing the vibration phenomenon are the reduced velocity $V_{ri} = u_0/(f_i d)$ ($i$ = either $x$ or $y$ depending on the dominant vibration mode) and the ratio of natural frequencies $f_{0x}/f_{0y}$. In order to exclude any implicit effect of fluid forces in the basic parameters and to facilitate engineering application, the ratio of natural frequencies $f_{0x}/f_{0y}$ was chosen as the basic parameter to describe the interaction of the two vibration modes. The horizontal vibration frequency $f_{0x}$, however, is strongly influenced by added mass effects due to the submergence of the gate (fluid forces proportional to the streamwise gate acceleration). For $f_{0x}/f_{0y} < 1.5$ the vibration frequencies $f_x$ and $f_y$ (i.e., the vibration frequencies caused by fluid excitation) will coincide (see below).

As mentioned in the Introduction, IIE mechanisms include ILEV-excitation and LEVS-excitation; see Figs. 2 and 3. The ILEV-excitation mechanism produces vibrations in the range $V_{ri} < 4$ with dominant amplitudes in the $x$ or $y$ direction depending on $V_{ri}$ (i.e., $x$-ILEV and $y$-ILEV, respectively). The LEVS-excitation mechanism leads to dominant streamwise excitation within the range $4.5 < V_{rx} < 7.5$. The mechanism only occurs if the instability of the shear layer deflecting from the leading edge of the gate lip is triggered by resonance of the gate itself. Thus, this mechanism will be called body-resonant leading-edge-vortex-shedding (BR-LEVS), as suggested in Billeter (1998) and Billeter and Staubli (2000). The cause of the BR-LEVS excitation mechanism was under discussion by various authors [e.g., Jongeling (1988) and Thang (1990)]; a possible explantion will be given in Section 5.2.

Regarding the adjacent mechanisms $y$-ILEV ($2 < V_{ry} < 4$) and BR-LEVS, the ratio of natural frequencies $f_{0x}/f_{0y}$ is of great significance. If $f_{0x}/f_{0y}$ is larger than 1.5, the gate response is quite similar to the response of a gate with only 1 d.o.f. With decreasing $f_{0x}/f_{0y}$, however, the excitation range of BR-LEVS is shifted towards smaller reduced velocities. If $f_{0x}/f_{0y}$ is smaller than $\approx 1.5$, the streamwise vibration frequencies $f_x$ becomes identical to the cross-flow vibration frequency $f_y$. The two excitation mechanisms will coincide, thus producing the maximum IIE-amplitudes and an extension of the ILEV-excitation range. Typical examples of both the dominant vibration amplitudes $y/d$ in the $y$-ILEV excitation range and of the dominant amplitudes $x/d$ in the BR-LEVS range are plotted versus the reduced velocities $V_{ry}$ and $V_{rx}$ in

Fig. 4. As mentioned above, the effect of the ratio of natural frequencies $f_{0x}/f_{0y}$ can clearly be seen. Fig. 4 also shows the typical behaviour of the mean lift coefficient $C_{Fy}$ and the mean contraction coefficient $C_c$ of the outflow, respectively. The sudden drop of $-C_{Fy}$ and $C_c$ at the upper end of the ILEV range results from the fact that beyond the ILEV range the interaction of the outflow shear layer with the trailing edge of the gate no longer occurs (see Sections 5.2–5.4). The main properties of the two excitation mechanisms ILEV and BR-LEVS which both belong to the class of IIE-mechanisms will be discussed subsequently.

### 5.2. *Pressure distribution along the gate lip*

In Fig. 5, typical distributions of the excitation coefficients $C^*_{pn}(i)$ deduced from the pressure measurements along the gate lip (see Fig. 1) are shown as a function of the streamwise distance from the leading edge of the gate ($x/d = 0$). The data of the pressure measurements at the vertical faces of the gate ($p_2, p_6, p_7$) are projected on the horizontal axis ($x/d = -0.25, 1.25, 1.5$). The $C^*_{pn}(i)$ give the instantaneous dimensionless pressure distribution along the gate lip when $i(t)$ is equal zero. If $C^*_{pn}(i) > 0$, energy is transferred from the flow to the gate vibration in the $i$ direction (dominant vertical excitation: $i(t) = y(t) = 0$; dominant streamwise excitation $i(t) = x(t) = 0$). Fig. 5 shows the $C^*_{pn}(x)$ of the mechanisms $x$-ILEV ($1.5 < V_{rx} < 2$), $y$-ILEV ($2 < V_{ry} < 4$) and BR-LEVS ($4 < V_{rx} < 7.5$). The following conclusions can be drawn.

(1) *Impinging-leading-edge-vortex (ILEV) excitation*. The pressure distribution along the gate lip has a wavy shape with dominant amplitudes towards the trailing edge ($p_5$ at $x/d = 0.75$). For the $x$-ILEV excitation the wavelength appears to be shorter than for the $y$-ILEV excitation. With increasing reduced velocities $V_{rx}$ and $V_{ry}$, the pressure gradient between the mid-lip position $p_4$ ($x/d = 0.5$) and the trailing edge position $p_5$ ($x/d = 0.75$) decreases for $x$-ILEV and increases for $y$-ILEV excitation; the waveform depends on $V_{rx}$, and $V_{ry}$, respectively. Dominant vertical excitation of $y$-ILEV occurs towards the trailing edge of the gate bottom ($p_5$), whereas the significant pressure fluctuation leading to horizontal $x$-ILEV can be located at the lower portion of the downstream face of the gate ($p_6$ at $x/d = 1.25$).

(2) *Body-resonant leading-edge-vortex-shedding (BR-LEVS) excitation*. The pressure distribution of the BR-LEVS excitation has a waveform with much smaller streamwise gradients along the gate bottom (i.e., between $0 < x/d < 1$) than the ILEV excitation. Significant pressure fluctuations at the trailing portion of the gate lip no longer occur. With increasing $V_{rx}$ the waveform is stretched and the wavelength grows.

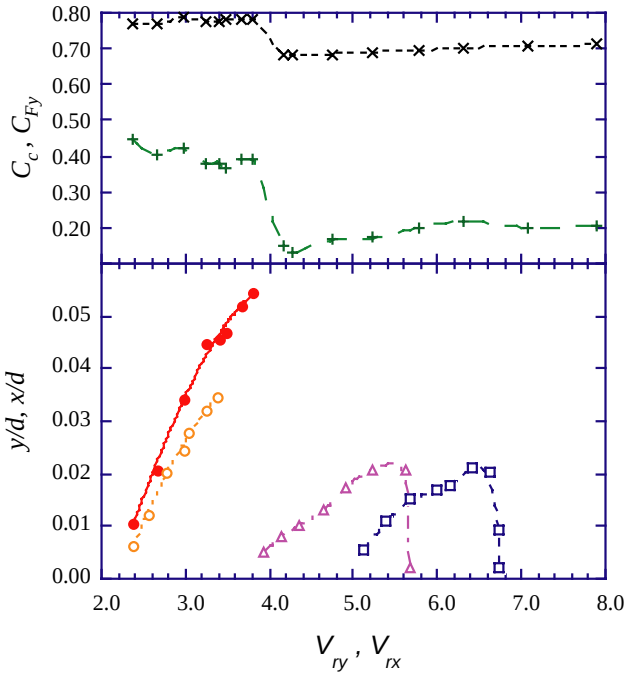


Fig. 4. Dominant relative amplitudes of the two excitation ranges: amplitudes $y/d$ of cross-flow ILEV with (•)$f_{0x}/f_{0y} = 1.0$ and (○) $f_{0x}/f_{0y} \to \infty$ (only 1 vertical d.o.f.); Amplitudes $x/d$ of streamwise BR-LEVS with (Δ) $f_{0x}/f_{0y} = 2.07$ and (□) $f_{0x}/f_{0y} \to 0$. Furthermore, the typical behaviour of the mean lift coefficient $C_{Fy}$ (- - + - -) and the contraction coefficient $C_c$ (┈ × ┈) are shown.

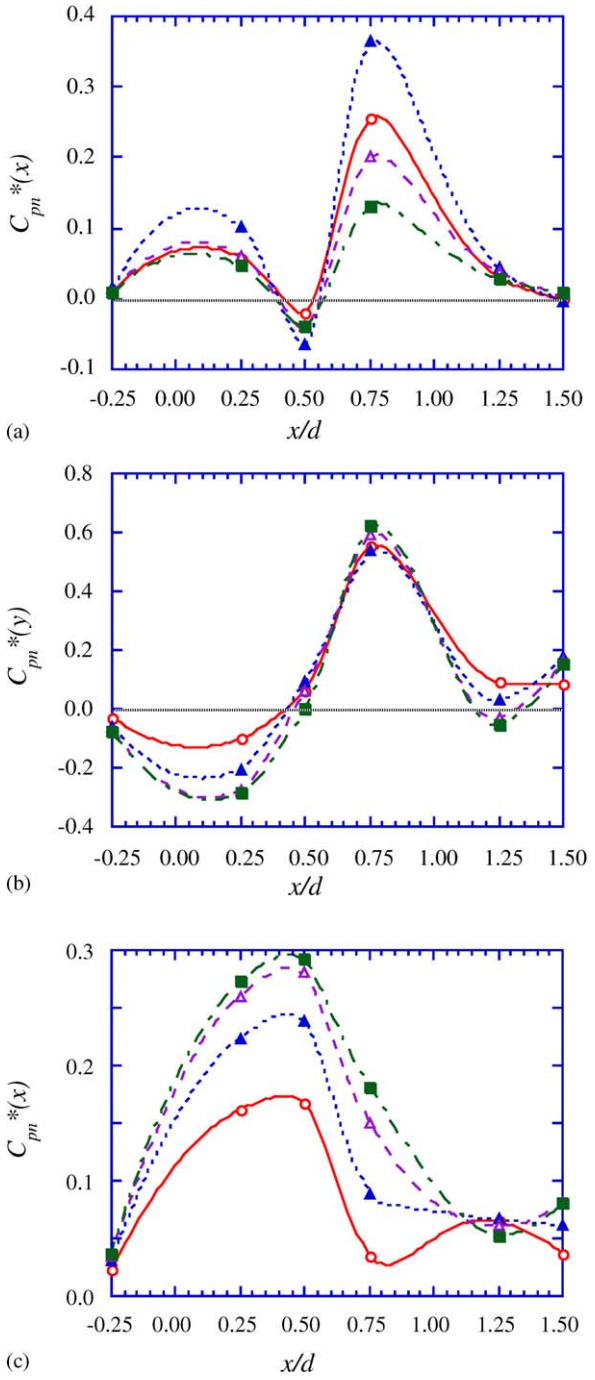


Fig. 5. Instantaneous pressure along the gate lip for the gate at equilibrium position ($x$-ILEV and BR-LEVS: $x(t)=0$, $y$-ILEV: $y(t)=0$): excitation coefficients $C_{pn}^*(i)$ according Eq. (4(b)). (a) $x$-ILEV: $f_{0x}/f_{0y} \to 0$, $s/d = 0.5$: $V_{rx} = 1.7$ (○), 1.8 (▲), 1.9 (Δ), 2.0 (■). (b) $y$-ILEV: $f_{0x}/f_{0y} > 1.5$, $s/d \approx 0.6$: $V_{ry} = 2.5$ (○), 3.0 (▲), 3.2 (Δ), 3.4 (■). (c) BR-LEVS: $f_{0x}/f_{0y} \to 0$, $s/d = 0.5$: $V_{rx} = 5.4$ (○), 5.7 (▲), 6.0 (Δ), 6.1 (■).

More detailed information on both the pressure distribution along the gate lip and the excitation coefficients $C_{pn}^*(i)$ for varying boundary conditions can be found in Billeter and Staubli (2000) and in Billeter (1998). However, some relevant properties of the excitation coefficients $C_{pn}^*(i)$ and the phase shifts $\varphi_{in}$ of the cross-flow ILEV and the

streamwise BR-LEVS mechanism will be pointed out. Therefore, the behaviour of the gate plate with 2 d.o.f. and a frequency ratio $f_{0x}/f_{0y} \approx 1.5$ will be considered. The ratio $f_{0x}/f_{0y} \approx 1.5$ marks some sort of limit value, below which the ILEV and the BR-LEVS mechanisms may coincide (the size of this limit value depends among other things on the added mass for the streamwise oscillation of the plate). By adjusting slightly the submergence of the gate, it was possible to produce a steady transition from the ILEV to the BR-LEVS excitation whilst the flow velocity $u_0$ and thus the reduced velocity $V_{ry} \approx V_{rx}$ were increased. In Fig. 6, the excitation (pressure) coefficients $C^*_{p2}(x)$, $C^*_{p5}(y)$, and $C^*_{p6}(x)$ as well as the phase shifts $\varphi_{x2}, \varphi_{y5}$ and $\varphi_{x6}$ between the deflection and the pressure fluctuations are plotted versus the reduced velocity ($p_2$ refers to the position of the pressure gauge at the upstream face, $p_5$ indicates the position near the trailing edge of the gate bottom and $p_6$ stands for the position at the downstream face of the plate, see Fig. 1). The following conclusions can be drawn.

(i) The vertical ILEV mechanisms is excited by maximum pressure fluctuations at the trailing edge. The phase shift between the vertical deflection and the pressure fluctuation at that position is close to $-90^\circ$ ($=-\pi/2$) indicating optimal excitation. Since the convection velocity $u_c$ of the ILEV flow structures can become as small as $0.2 \times u_0$ (see Fig. 7(a) and 10: $u^*_c \to 0.2$), the theoretical maximum of $C^*_{pn}(y)$ is $C^*_{pn}(y) = 1 - (u^*_c)^2 = 0.96$, a value which is nearly reached by the $C_{p5}(y)$ in Fig. 6(a).

(ii) Although some excitation in the streamwise direction is caused by pressure variations in the headwater of the gate [this excitation vanishes for $f_{0x}/f_{0y} \approx 1$ when the ILEV and BR-LEVS mechanisms coincide; see Billeter (1998)], the dominant excitation of streamwise BR-LEVS vibrations occurs at the lower portion of the downstream (i.e., tailwater) face of the gate plate (compare $C^*_{p2}(x)$ and $C^*_{p6}(x)$ in Fig. 6(a)). In the BR-LEVS range the phase shift $\varphi_{x6}$ decreases steadily with increasing reduced velocities $V_{rx}$. As further explained in Sections 5.3 and 5.4, this behaviour points out the convective nature of the flow structure causing the BR-LEVS mechanism.

### 5.3. Properties of the relevant flow structures

Subsequently, we will focus on the characteristic properties of the pressure distribution (i.e., the pressure wave along the gate bottom). Assuming the pressure $p(x, t)$ as given in Eq. (2), the convection velocity $u^*_c$, wavelength $\lambda^*$ and spatial growth rate $-k^*_j$ can be computed from the pressure measurements $p_3$, $p_4$ and $p_5$ along the gate bottom as shown in Eq. (5). Figs. 7–9 show the relevant $u^*_{c,nm}$, $\lambda^*_{nm}$ and $-k^*_{j,nm}$ plotted versus $V_{ry}$ and $V_{rx}$, respectively. The index "*nm*" stands for the positions between which the $u^*_{c,nm}$, $\lambda^*_{nm}$ and $-k^*_{j,nm}$ were computed according to Eqs. (5a)–(5c). The index "34" indicates the properties along the upstream part of the gate bottom, index "45" stands for the properties along the downstream part towards the trailing edge and index "35" is appended to the average properties along the gate lip. We investigate the vertical ILEV and the horizontal BR-LEVS excitation and compare the $u^*_{c,nm}$, $\lambda^*_{nm}$ and $-k^*_{j,nm}$ of gates with either 1 or 2 d.o.f.

Above all, we found that the functions $u^*_{c,nm}(V_{ri})$, $\lambda^*_{nm}(V_{ri})$ and $-k^*_{j,nm}(V_{ri})$ depend on both the excitation mechanism considered and the position for which they were computed. Furthermore, $u^*_{c,nm}$, $\lambda^*_{nm}$ and $-k^*_{j,nm}$ are considerably influenced by the number of d.o.f. of the vibrating structure. The relevant findings can be summarized as follows.

(1) *Impinging-leading-edge-vortex (ILEV) excitation*. At the beginning and in the middle of the excitation range ($2.2 < V_{ry} < 3$) the convection velocity $u^*_c$ increases in the streamwise direction. This behaviour can be explained by the strong streamwise mean pressure gradient of the discharge under the gate. The $u^*_{c,45}$ towards the trailing edge of the gate, however, decreases strongly with increasing $V_{ry}$, so that at the upper end of the excitation range the value of $u^*_c$ is nearly constant along the gate bottom ($u^*_c \approx 0.2$). The same findings hold for the wavelength and even the growth rate: whereas $\lambda^*$ and $-k^*_j$ have a strong gradient in the streamwise direction at the beginning of the excitation range, they tend towards constant values along the gate bottom at the upper end of the $V_{ry}$-range (we could say that the instability wave becomes compressed with increasing $V_{ry}$). The assumption of a pressure distribution according to Eq. (2) holds, strictly speaking, only at the upper end of the excitation range. In this range the excitation produces the maximum vibration amplitudes. In other terms: the final state of the excitation mechanism is associated with a harmonic pressure distribution along the gate bottom and with a constant growth rate of the pressure amplitude. The excitation mechanism can be explained as follows [see also Thang (1990)]: the first flow instability of the shear layer with $\mathrm{Sh}_1 \approx 0.4$ ($V_{ry} = 2.5$) is amplified by the interaction with the trailing edge of the gate (shear layer impingement) and sustained by the closed feedback-loop consisting of the flow instability and the gate motion. At the beginning of the excitation ($V_{ry} < 2.5$, small amplitudes) the properties of shear layer instability are influenced by the mean pressure gradient of the discharge. At the upper end of the $V_{ry}$-range the mechanism is fully developed. At this stage both the properties of the pressure wave along the gate bottom and the propagation of the coherent structures in the shear layer follow the assumptions of the linear stability theory [see Martin et al. (1975)]. Comparing the oscillators with 1 and 2 d.o.f., we can conclude that the presence of a second (horizontal) d.o.f. with the natural frequency $f_{0x}$ close to the natural frequency

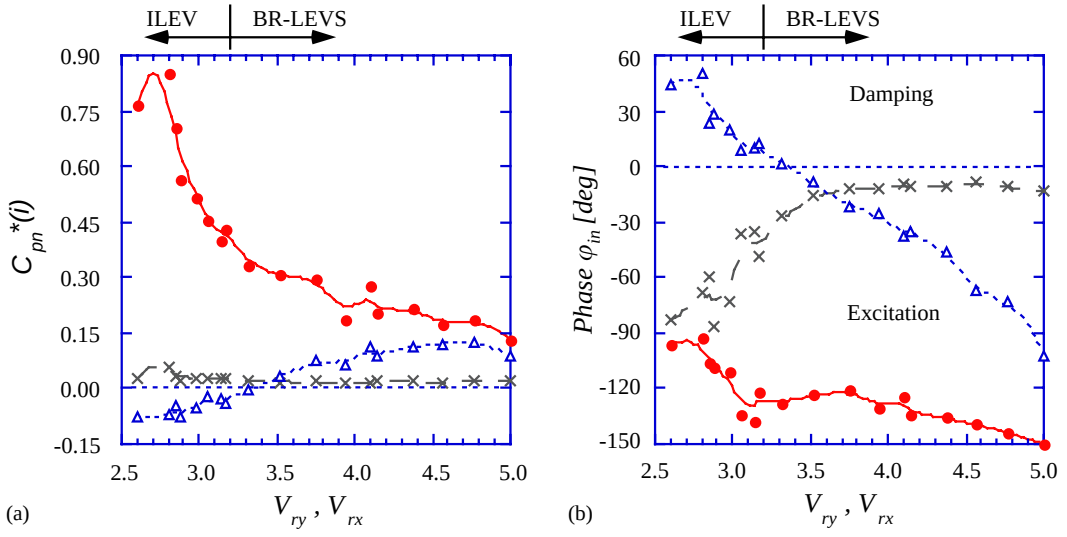


Fig. 6. Transition from cross-flow ILEV to streamwise BR-LEVS for the gate with 2 d.o.f. and $f_{0x}/f_{0y} = 1.47$. (a) Excitation coefficients: ($\times$) $C_{p2}^*(x)$, ($\bullet$) $C_{p5}^*(y)$ and ($\Delta$) $C_{p6}^*(x)$. (b) Phase shift $\varphi_{in}$ between deflection and pressure: ($\times$) $\varphi_{x2}$, ($\bullet$) $\varphi_{y5}$ and ($\Delta$) $\varphi_{x6}$.

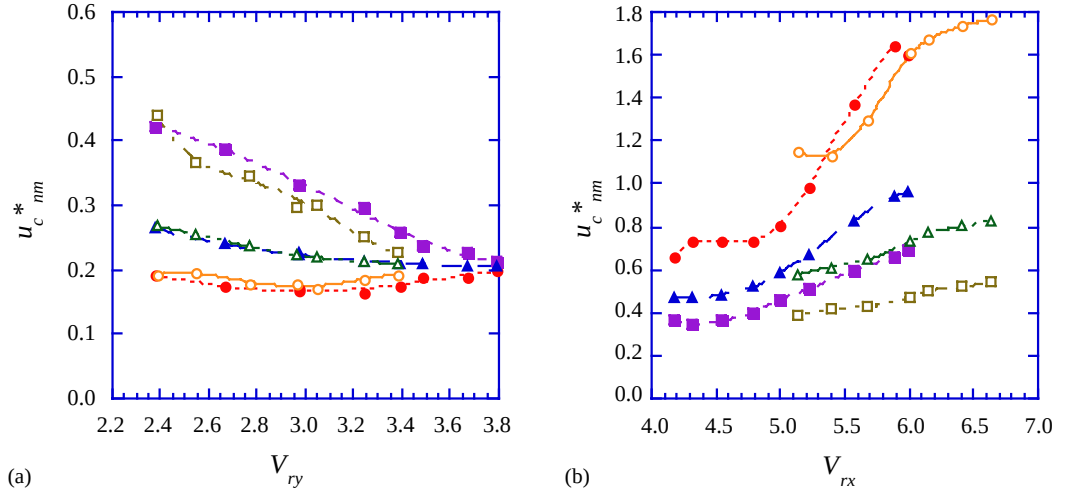


Fig. 7. Convection velocity $u_c^*$ of the pressure wave along the gate lip (Eq. (5c)) plotted versus the reduced velocities $V_{ry}$ or $V_{rx}$. (a) $y$-ILEV excitation; open signs: 1 d.o.f., $f_{0x}/f_{0y} \to \infty$, solid signs: 2 d.o.f., $f_{0x}/f_{0y} = 1.0$. (b) BR-LEVS excitation; open signs: 1 d.o.f., $f_{0x}/f_{0y} \to 0$, solid signs: 2 d.o.f., $f_{0x}/f_{0y} = 2.46$. ($\bigcirc$,$\bullet$) $u_{c,34}^*$, ($\square$,$\blacksquare$)$u_{c,45}^*$, ($\Delta$,$\blacktriangle$) $u_{c,35}^*$.

$f_{0y}$ of the vertical d.o.f. ($0.9 < f_{0x}/f_{0y} < 1.5$) enhances the tendency of the mechanism to reach the final stage of the excitation (and thus extends the excitation range).

Finally, it should be mentioned that the mean wavelength $\lambda^*$ is always smaller than 1 ($\lambda < d$). In Fig. 10, the average $u_c^*$ and $\lambda^*$ of the horizontal ($x$-) ILEV excitation are plotted together with the data of the vertical ($y$-) ILEV mechanism. Furthermore, the significant term $(n + \varepsilon)$ representing the phase condition of the shear layer impingement (Eq. (5d)) is added.

Taking into account that the properties shown in Fig. 10 are rough estimates computed from the pressure measurements at $x/d = 0.25$ and $x/d = 0.75$, the following *phase conditions* can be deduced as intrinsic features of the ILEV-excitation in the vertical (cross-flow, $y$) and the horizontal (streamwise, $x$) direction, respectively: for $y$-ILEV, $d/\lambda = (n + \varepsilon)$ with $0 < \varepsilon < 0.5$ and for $x$-ILEV, $d/\lambda = (n + \varepsilon)$ with $-0.5 < \varepsilon < 0$.

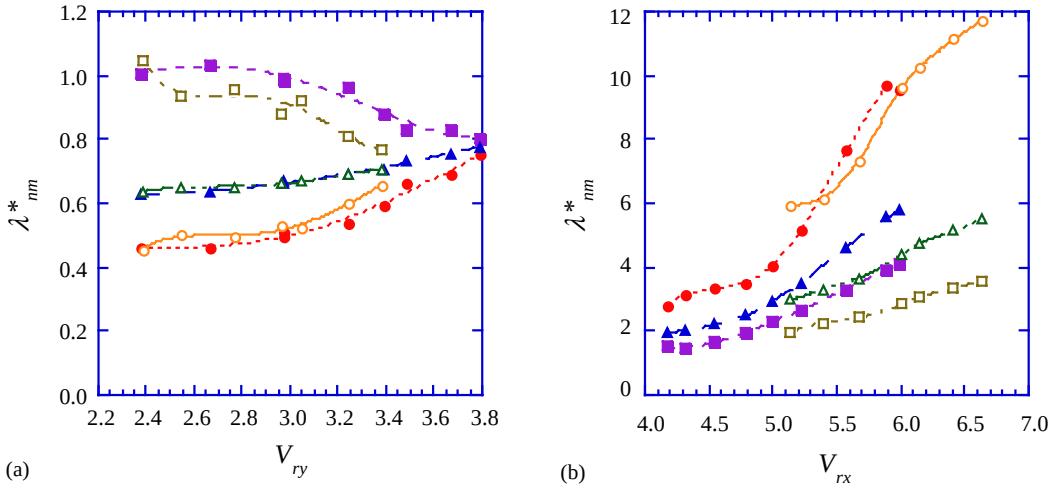


Fig. 8. Wavelength $\lambda^*$ of the pressure wave along the gate lip (Eq. (5a)) plotted versus the reduced velocities $V_{ry}$ or $V_{rx}$. (a) $y$-ILEV excitation; open signs: 1 d.o.f., $f_{0x}/f_{0y} \to \infty$, solid signs: 2 d.o.f., $f_{0x}/f_{0y} = 1.0$. (b) BR-LEVS excitation; open signs: 1 d.o.f., $f_{0x}/f_{0y} \to 0$, solid signs: 2 d.o.f., $f_{0x}/f_{0y} = 2.46$. (○,●)$\lambda^*_{34}$, (□,■)$\lambda^*_{45}$, (Δ,▲) $\lambda^*_{35}$.

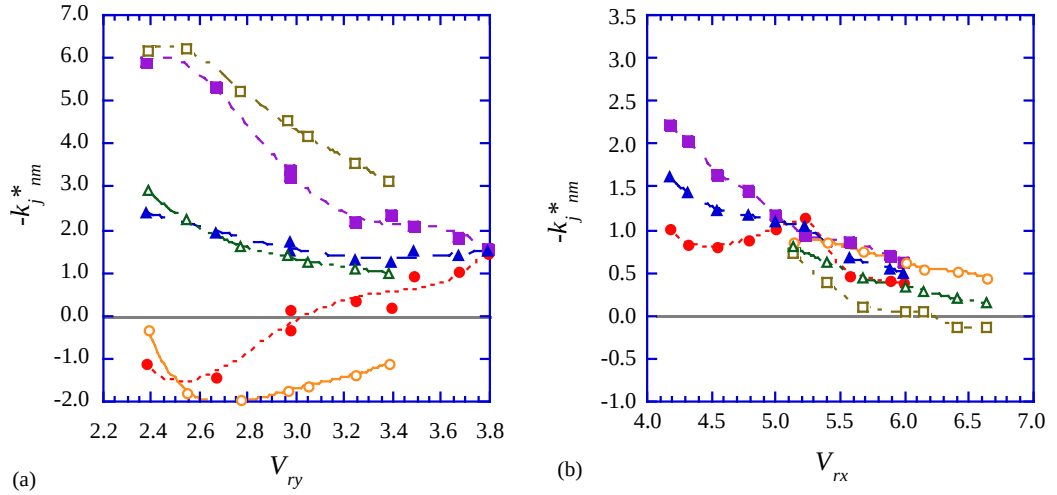


Fig. 9. Spatial growth rate $-k^*_j$ of the pressure wave along the gate lip (Eq. (5b)) plotted versus the reduced velocities $V_{ry}$ or $V_{rx}$. (a) $y$-ILEV excitation; open signs: 1 d.o.f., $f_{0x}/f_{0y} \to \infty$, solid signs: 2 d.o.f., $f_{0x}/f_{0y} = 1.0$. (b) BR-LEVS excitation; open signs: 1 d.o.f., $f_{0x}/f_{0y} \to 0$, solid signs: 2 d.o.f., $f_{0x}/f_{0y} = 2.46$. (○,●) $-k^*_{j,34}$, (□,■) $-k^*_{j,45}$, (Δ,▲) $-k^*_{j,35}$.

(2) *Body-resonant leading-edge-vortex-shedding (BR-LEVS) excitation*. Both the convection velocities and the wavelengths decrease towards the tailwater of the gate ($u^*_{c,45} < u^*_{c,34}, \lambda^*_{45} < \lambda^*_{34}$). This behaviour is very similar to the development of the approach flow upstream of the onset of vortex formation in a plane shear layer. At the beginning of the excitation range the mean convection velocity is close to the convection velocity of the shear layer separating from the rigid gate ($u^*_c \approx 0.6$, Section 4). From the wavelength $\lambda^*$ which is always larger than $\lambda^* \approx 2$, we can deduce that the vortex formation will only start in the tailwater downstream of the trailing edge of the gate. With increasing $V_{rx}$ both the mean convection velocities and the wavelengths increase as well: it seems as if the instability wave is stretched towards the upper end of the excitation range. For the gate with 1 d.o.f. the excitation starts at $V_{rx} \approx 5$. This $V_{rx}$ corresponds to the dimensionless frequency $\mathrm{Sh}_2 \approx 0.2$ of the second vortex in the shear layer beneath the rigid gate. Together with the behaviour of the excitation coefficients $C_{pn}{}^*(x)$, these findings lead to the following conclusion: the excitation mechanism is primarily caused by the second instability wave of the efflux shear layer. The excitation is only effective if the instability is enhanced and triggered by the elastic motion of the separation point of the shear layer (i.e.,

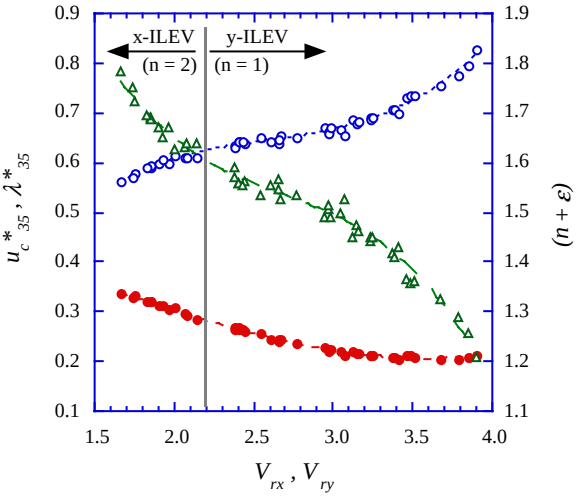


Fig. 10. Intrinsic features of ILEV-excitation: •, $u^*_{c,35}$; ○, $\lambda^*_{35}$; Δ, $(n + \varepsilon)$; all plotted versus $V_{ri}$.

the leading edge of the gate): a positive feedback-loop only exists if the flow instability is coupled with a streamwise motion of the gate. Following Monkewitz and Nguyen (1987), we can argue that the instability wave which is convectively unstable when separating from a rigid body becomes absolutely unstable (with resonance of the upstream and downstream instability waves) when coupled to an elastic body with appropriate vibration modes. The explanation given above describes a proper excitation mechanism for the streamwise vibration within the range $4 < V_{rx} < 7.5$. This mechanism is called BR-LEVS, as mentioned before. It is produced by the instability of the shear layer in the tailwater and not by the interaction of the shear layer with the trailing edge of the gate.

The growth rate $-k_j^*$ of the BR-LEVS excitation will not be discussed in detail since it has only limited relevance to the vibration amplitudes (the dominant excitation occurs at the tailwater face of the gate). However, it should be mentioned that the $-k_j^*$ of the BR-LEVS instability is much smaller than the growth rate of the ILEV mechanism. Furthermore, we find that $-k_j^*$ is nearly constant along the gate bottom at $V_{rx} = 1/\mathrm{Sh}_2 \approx 5$ where the BR-LEVS excitation of the gate with 1 d.o.f. starts.

The effect of a second d.o.f. on BR-LEVS excitation is considerable and can be summarized as follows. For structures with 2 d.o.f., the excitation range is shifted towards smaller $V_{rx}$. With decreasing $f_{0x}/f_{0y}$, the excitation range gradually approaches the ILEV-excitation range. At the same time, both the wavelength $\lambda^*$ and the convection velocity $u_c^*$ decrease whereas the growth rate at the trailing part of the gate lip increases strongly. For gates with 2 d.o.f. and the ratio of natural frequencies in the range $0.9 < f_{0x}/f_{0y} < 1.5$, the BR-LEVS excitation interacts positively with the ILEV mechanism. The ILEV-excitation range is extended towards larger $V_r$ and the maximum amplitudes caused by IIE are achieved (Billeter, 1998).

### 5.4. Flow field in the tailwater

Further evidence for the distinct behaviour of both the ILEV excitation and the BR-LEVS excitation can be deduced from the velocity measurement in the tailwater of the gate. In Fig. 11, the cross-correlation between the dominant pressure fluctuations at the gate and the cross-flow velocity in the tailwater is plotted for increasing streamwise distance between the locus of flow separation at the gate ($x/d = 0$) and the location of the velocity measurement. The correlation time is written in dimensionless form as $V_r(\tau) = u_0\tau/d$. In the cross-correlation $R_{p5,v}(t)$ of the ILEV excitation, we find strongly periodical structures with a dimensionless period of $V_r(\tau) \approx 3.4$ only beneath the trailing edge of the gate ($x/d = 0.9$). With increasing distance between the gate and the velocity measurement point, this periodical component diminishes whilst a second periodical structure with $V_r(\tau) \approx 6.8$ evolves. In the cross-correlation $R_{p6,v}(\tau)$ of the BR-LEVS excitation, however, only one significant structure with a dimensionless period of $V_r(\tau) \approx 5$ can be found. This structure remains persistent over the whole range of $x/d$ measured. It is independent of the streamwise separation between the pressure and the velocity measurement. This specific behaviour indicates that the ILEV excitation is a local phenomenon which occurs close to the trailing edge of the gate, whereas the BR-LEVS excitation is caused by flow instabilities with larger spatial extensions towards the tailwater of the gate.

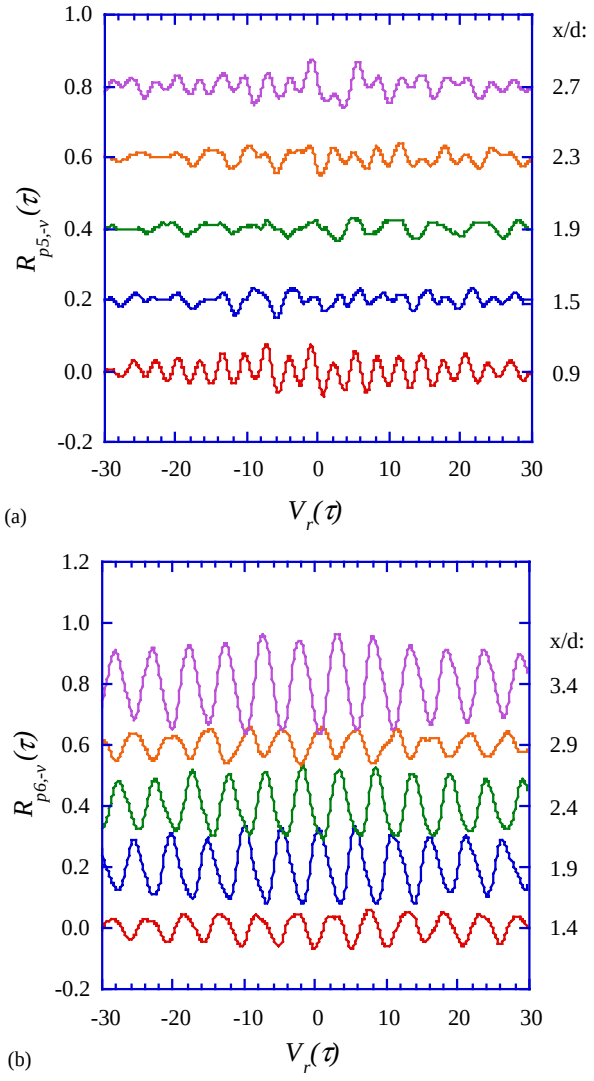


Fig. 11. Cross-correlation of boundary pressure and cross-flow velocity $v(t)$ measured for increasing streamwise distance $x/d$. (a) $y$-ILEV: $R_{p5,-v}(\tau)$, (b) BR-LEVS: $R_{p6,-v}(\tau)$ (see also Fig. 12).

These findings are confirmed by the power spectra $S_{v,v}(f)$ of the cross-flow velocity $v(t)$ measured for increasing streamwise distance from the gate. The spectra in Fig. 12 are plotted versus the dimensionless frequency $\mathrm{Sh}(f) = fd/u_0$. In the spectra of the ILEV excitation (Fig. 12(a)) we find two dominant peaks. The peak with the higher frequency (which is the vertical vibration frequency of the gate) belongs to the ILEV instability and it becomes weaker with increasing $x/d$. The second peak with a lower frequency, however, increases with increasing $x/d$. The flow instability producing the lower dominant frequency in the ILEV spectra (Fig. 12(a)) is the same as the one being responsible for the BR-LEVS excitation. The flow structure caused by this instability is persistent over a wide range in the tailwater of the gate. In the spectra of the BR-LEVS excitation (Fig. 12(b)) we consequently find one dominant peak at the horizontal vibration frequency (and some higher harmonics) and the spectral density $S_{v,v}(f)$ of this peak remains nearly constant over the whole range of $x/d$ investigated.

Both the findings of Section 5.3 and the analysis of flow velocity measurements in the tailwater of the gate lead to the conclusion that two different flow patterns and two different types of flow structure interactions generate the two excitation mechanisms ILEV and the BR-LEVS (see Fig. 3). The ILEV mechanism is caused by the local interaction of the shear layer underneath the gate plate with the trailing edge of the gate lip. The BR-LEVS mechanism is produced by the instability of the shear layer in the tailwater of the gate, with the instability being necessarily triggered by the elastic

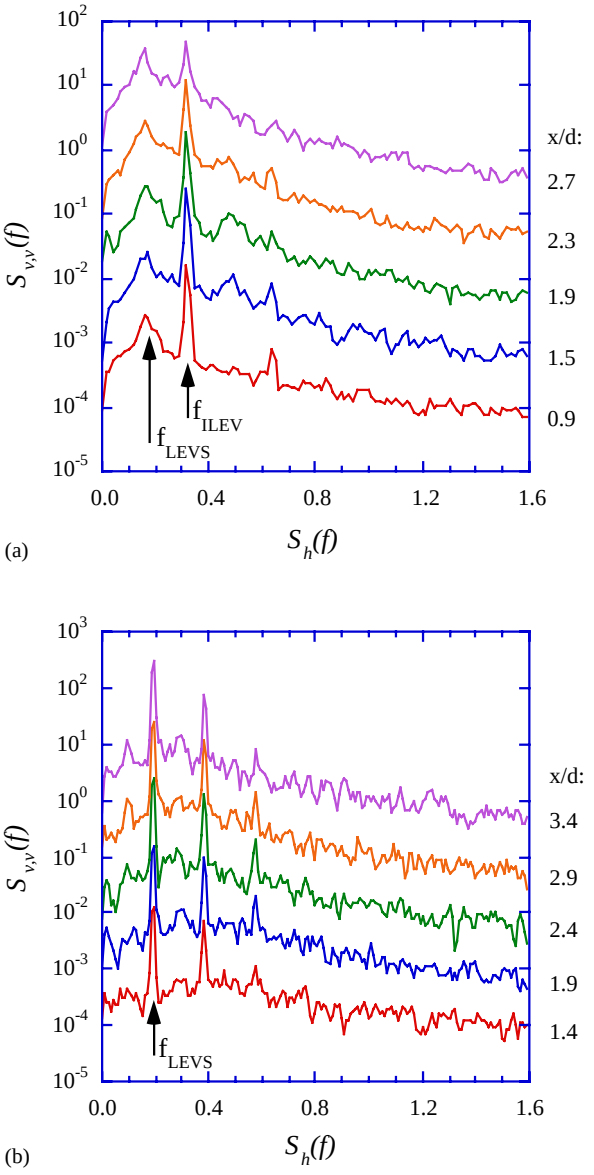


Fig. 12. Power spectra $S_{v,v}(f)$ of the cross-flow velocity $v(t)$ measured for increasing streamwise distance $x/d$ from the gate. (a) $y$-ILV, 2 d.o.f, $f_{0x}/f_{0y} = 1.54$, (b) $x$-BR-LEVS, 1 d.o.f.

motion of the flow separation at the leading edge of the gate. Within a limited range of the ratio of natural frequencies of $0.9 < f_{0x}/f_{0y} < 1.5$ the two mechanism (and consequently, the two flow patterns and the two types flow structure interactions, respectively) will coincide and interact positively, thus producing both maximum excitation and response amplitudes.

## 6. Conclusion

The instability of a single shear layer separating from a rectangular elastic body was investigated experimentally using a gate plate with 2 d.o.f. and submerged discharge. It was shown that two types of flow instabilities exist in the flow field downstream of the flow separation: (a) an instability which is caused by the interaction of the shear layer with the

trailing edge of the body, and (b) an instability of the shear layer in the tailwater of the gate, the latter being effective only when coupled to the elastic motion of the flow separation at the leading edge of the body (Fig. 3).

Both of these instabilities may cause flow-induced vibrations: the local instability between the leading and the trailing edge of the body is the major source of cross-flow and streamwise impinging-leading-edge-vortex (ILEV) excitation; the flow instability in the tailwater leads to streamwise body-resonant leading-edge-vortex-shedding (BR-LEVS) excitation.

## Acknowledgements

Financial support provided by the Swiss Federal Institute of Technology (ETHZ) and the Laboratory of Hydraulics (VAW) is gratefully acknowledged.

## References

Billeter, P., 1998. Strömungsinduzierte Schwingungen von Schützen mit mehreren Freiheitsgraden. VAW Mitteilung 125, VAW-ETH Zurich (in German).

Billeter, P., Staubli, T., 2000. Flow-induced multiple mode vibrations of gates with submerged discharge. Journal of Fluids and Structures 14, 323–338.

Hardwick, J.D., 1974. Flow-induced vibrations of vertical-lift gate. ASCE Journal of Hydraulic Division 100/HY5, 631–644.

Ho, C-M., Huerre, P., 1984. Perturbed free shear layers. Annual Review of Fluid Mechanics 16, 365–424.

Ishii, N., Knisely, C.W., 1990. Shear layer behaviour under a streamwise vibrating gate and its significance to gate vibration. JSME International Journal (S III) 33/2, 131–138.

Jongeling, T.H., 1988. Flow-induced self-excited in-flow vibrations of gates. Journal of Fluids and Structures 2, 541–566.

Kolkman, P.A., 1976. Flow-induced gate vibrations. Delft Hydraulics Laboratory Publication, No. 164.

Martin, W.W., Naudascher, E., Mahgadevan, P., 1975. Fluid-dynamic excitation involving flow instability. ASCE Journal of Hydraulic Division 101/HY6, 681–698.

Monkewitz, P.A., Nguyen, L.N., 1987. Absolute instability in the near-wake of two-dimensional bluff bodies. Journal of Fluids and Structures 1, 165–184.

Naudascher, E., Rockwell, D., 1994. Flow-induced Vibrations—an Engineering Guide; IAHR Hydraulic Structures Design Manual, A.A. Balkema, Rotterdam.

Thang, N.D., 1990. Gate vibrations due to unstable flow separation. ASCE Journal of Hydraulic Engineering 116/HY3, 342–361.

Thang, N.D., Naudascher, E., 1986. Self-excited vibrations of vertical lift gates. IAHR Journal of Hydraulic Research 24, 391–404.